

Correlation between the ionizing continuum and variable C iv broad absorption line in multi-epoch observations of SDSS J141007.74+541203.3

Hong-Yan Huang,¹* Cai-Juan Pan,²* Wei-Jian Lu,³ Yi-Ping Qin,⁴ Ying-Ru Lin,³ Wei-Rong Huang,⁴ Yu-Tao Zhou,^{5,6} Min Yao,³ Wei-Jing Nong,² Mei-Mei Lu,² Zhi-Kao Yao² and Qing-Lin Han²

¹*School of Physics and Electronic Information, Yunnan normal University, Kunming 650500, China*

²*School of Materials Science and Engineering, Baise University, Baise 533000, China*

³*School of Information Engineering, Baise University, Baise 533000, China*

⁴*Center for Astrophysics, Guangzhou University, Guangzhou 510006, China*

⁵*Key Laboratory of Optical Astronomy, National Astronomical Observatories, Chinese Academy of Sciences, Beijing 100012, China*

⁶*University of Chinese Academy of Sciences, Beijing 100049, China*

Accepted 2019 XXX. Received 2018 YYY; in original form 2018 ZZZ

ABSTRACT

Correlation between the variations of quasar absorption lines and the ionizing continuum have been recently confirmed in systematic studies. However, no convincing individual case is reported. We present a statistical analysis of the variable C iv broad absorption line (BAL) in the quasar SDSS J141007.74+541203.3, which have been observed with 44 epochs by the Sloan Digital Sky Survey Data Release 14. Grier et al. (2015) has recently concluded that the most likely cause of the variability of the BAL in SDSS J141007.74+541203.3 is a rapid response to changes in the incident ionizing continuum. In this paper, we confirm the anticorrelation between the equivalent width of BALs and the flux of the continuum based on the spectra of this quasar that show significant variations, which serve as another independent evidence for the view of Grier et al. (2015).

Key words: galaxies: active–quasars: absorption lines–quasars: individual (SDSS 141007.74+541203.3).

1 INTRODUCTION

Quasars are the brightest and densest objects in the active galactic nucleus (AGNs). It is believed that the intrinsic absorption lines are generated by the high-velocity flowing wind and emitted near the supermassive black hole (SMBH) of the quasar. With respect to the full width at half maximum (FWHM, which also be known as width of absorption lines) of line spread, the intrinsic absorption lines are classified as three types: broad absorption lines (BALs) with $\text{FWHM} \geq 2000 \text{ km s}^{-1}$ (e.g. Weymann et al. 1991; Hamann et al. 2008); mini-BALs with $2000 > \text{FWHM} > 500 \text{ km s}^{-1}$ (e.g. Misawa et al. 2007b; Ganguly & Brotherton 2008); narrow absorption lines (NALs) with $\text{FWHM} \leq 500 \text{ km s}^{-1}$ (e.g. Misawa et al. 2007a, 2014).

The outflowing winds revealed by intrinsic absorption

lines in quasar spectra are important at least for the following two reasons. First, the BALs can be observed in ~ 41 per cent of optically observed quasars (e.g. Allen et al. 2011), this observed frequency indicates that outflowing winds play a significant role in the nuclear environment (e.g. Crenshaw et al. 2003). Second, as a form of feedback from the quasars into massive galaxies, quasar outflowing winds could remove cold gas and thus regulate star formation and more SMBH accretion (e.g. Springel et al. 2005; King 2010).

The variation of BALs is a powerful tool for studying the properties of the outflowing gas, such as the size, kinematics, material composition and evolution. The reason for the variations of BAL with time is generally considered to be the transverse motion of the gas (e.g. Hamann et al. 2008; Shi et al. 2016; Hemler et al. 2019) or the ionization variation of the outflowing gas (e.g. Grier et al. 2015; Lu et al. 2017; Lu et al. 2018; Hemler et al. 2019). Whichever of the above two reasons, BAL variation on short time-scales can

* E-mail: 936499587@qq.com (H-Y, H); pancj2017@126.com (C-J, P)

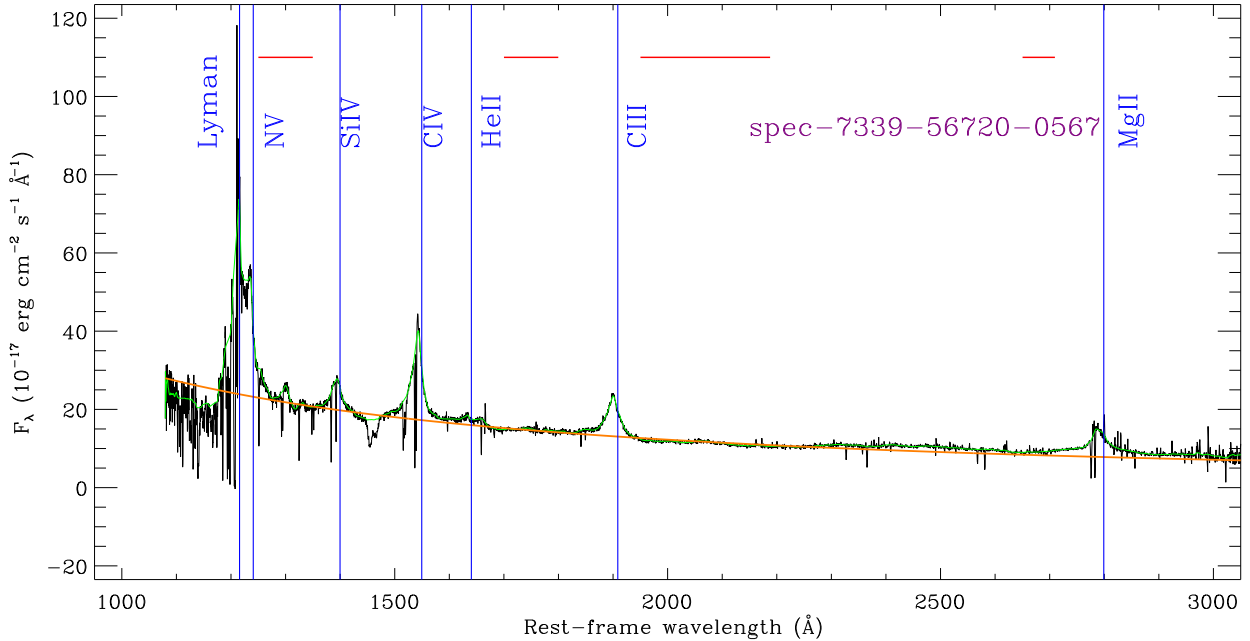


Figure 1. The continuum fitting of SDSS J1410+5412 (on MJD 56720). The blue verticals mark the emission lines. The black curve is the original spectrum from the SDSS. The orange curve is the power-law continuum fitting. The green curve is the pseudo-continuum spectrum. The red horizontal lines are the relatively line-free wavelength regions (1250–1350, 1700–1800, 1950–2200, and 2650–2710 Å in the rest frame) for continuous iterative fitting.

be used to measure the distance of the absorber from the central SMBH. Shorter variation time-scales indicate smaller distances. In the traverse scenario, shorter variation time-scales indicate shorter crossing times of the outflowing clouds (Hamann et al. 2008; Capellupo et al. 2011); while in the ionization change scenario, shorter variation time-scales represent shorter recombination times, which indicates the higher densities of the clouds (Hamann et al. 1997). In addition, whether there is variability on longer (several years) time-scales indicates whether the outflowing gas has a persistent structure. Furthermore, variability studies of BAL, mini-BAL and intrinsic NAL can address the evolution of outflows. In an evolution model (e.g. Farrah et al. 2007), these three types of absorption lines represent different evolution phases of the outflows. The BAL may be the powerful phase of the outflowing wind, while the other two types of absorption lines may appear at its beginning or the ending stages (e.g. Hamann et al. 2008).

Correlation studies between the continuum and the variations of absorption lines have been proposed to investigate the variability reason of absorption lines. Actually, some researches on the correlation between the variations of BALs and the persistence/radiation have been carried out. A few works have reported that no apparent correlations between the variations of BALs and that of the continuum (e.g. Gibson et al. 2008; Wildy et al. 2014; Vivek et al. 2014), but several recent studies have provided evidence of anticorrelations between the variations of absorption lines and the continuum (e.g. Lu et al. 2018; Lu & Lin 2018b for BAL; Lu et al. 2017; Chen et al. 2018b,a for NAL).

The above-mentioned works are based on the anal-

ysis of multiple sources. A particular quasar SDSS J141007.74+541203.3 ($z_{\text{em}} = 2.35$; Hewett & Wild (2010), hereafter J1410+5412) with multi-epoch observations was explored in detail by Grier et al. (2015) and Hemler et al. (2019). A linear speed with 4340 km s^{-1} in rapidly variations of its CIV BALs was reported, which is seem to be caused by a rapid response to changes in the incident ionizing continuum. It is interesting to find out whether there is a correlation between the variations of CIV BAL and the flux of the continuum in J1410+5412. The paper is structured as follows. In Section 2, we describe characteristics and analysis of the data. The correlation analysis and discussion will be given in Section 3, where also including a brief summary. The cosmological parameters used in this article are $\Omega_{\text{M}} = 0.3$, $\Omega_{\Lambda} = 0.7$, $H_0 = 70 \text{ km s}^{-1} \text{ Mpc}^{-1}$.

2 SPECTRAL ANALYSIS

The quasar J1410+5412 studied in this paper is a target of the Sloan Digital Sky Survey Reverberation Mapping Project (SDSS-RM; Shen et al. 2015), the latter is a dedicated multi-target reverberation mapping campaign performed as part of SDSS-III (Eisenstein et al. 2011) BOSS survey (Dawson et al. 2013). A technical overview of the SDSS-RM project could be seen in Shen et al. (2015). The apparent *i*-band magnitude of the quasar is $m_i = 18.1$ (Alam et al. 2015). The average value of the Signal to Noise Ratio (S/N) of the spectra is 26.60 (22.23~37.54), there are listed in Table 1. The spectrograph has wavelengths from 3650 to 10400 Å and a spectral resolution

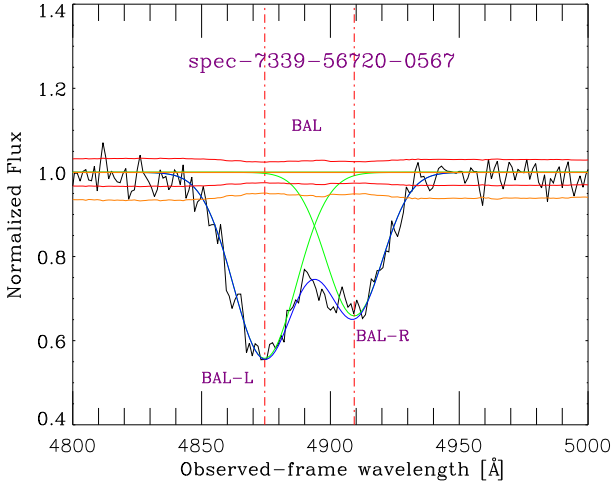


Figure 2. The fitting for the C iv BAL in SDSS J1410+5412 (on MJD 56720). The black curve is the original spectrum from the SDSS. The orange thick line is pseudo-continuum-normalized spectrum; the red and orange curves are the uncertainty levels that have been normalized by the corresponding pseudo-continua; the red vertical dotted lines are the center of the BAL-L and BAL-R trough, respectively; the green curves are the Gaussian fittings for the BAL-L and BAL-R trough; the blue curves are multiple Gaussian fittings for them.

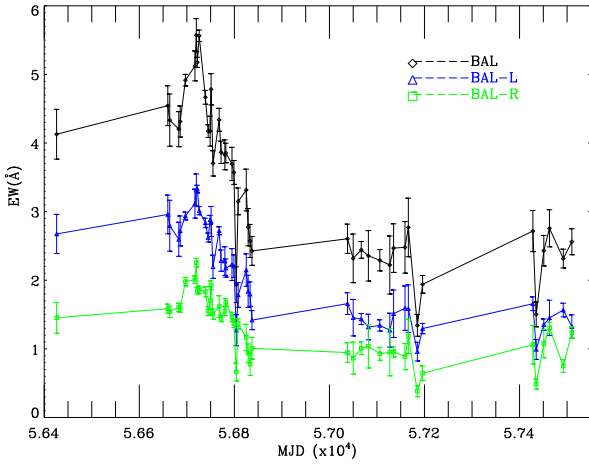


Figure 3. The EW of the BALs versus the time within MJD=56426~57510 (in the rest frame). The black, blue and green curves are the EWs of BAL, BAL-L, and BAL-R, respectively.

of $R \sim 2000$ (Smeed et al. 2013). We collect 44-epoch spectra of SDSS J1410+5412 from the Data Release 14 (DR14, Abolfathi et al. 2018). The time of these observations cross from MJD 56426 to 57510.

To evaluate the variation of the continuum, we fitted each spectrum of SDSS J1410+5412 using a power-law function. The power-law continuum was iteratively fitted in several wavelength regions (1250–1350, 1700–1800, 1950–2200, 2650–2710 Å in the rest frame), which are defined by Gibson et al. (2009) as “relatively line-free (RLF) regions”. During the fitting, we ignored the pixels beyond 3σ significance for reducing the influences of emission/absorption

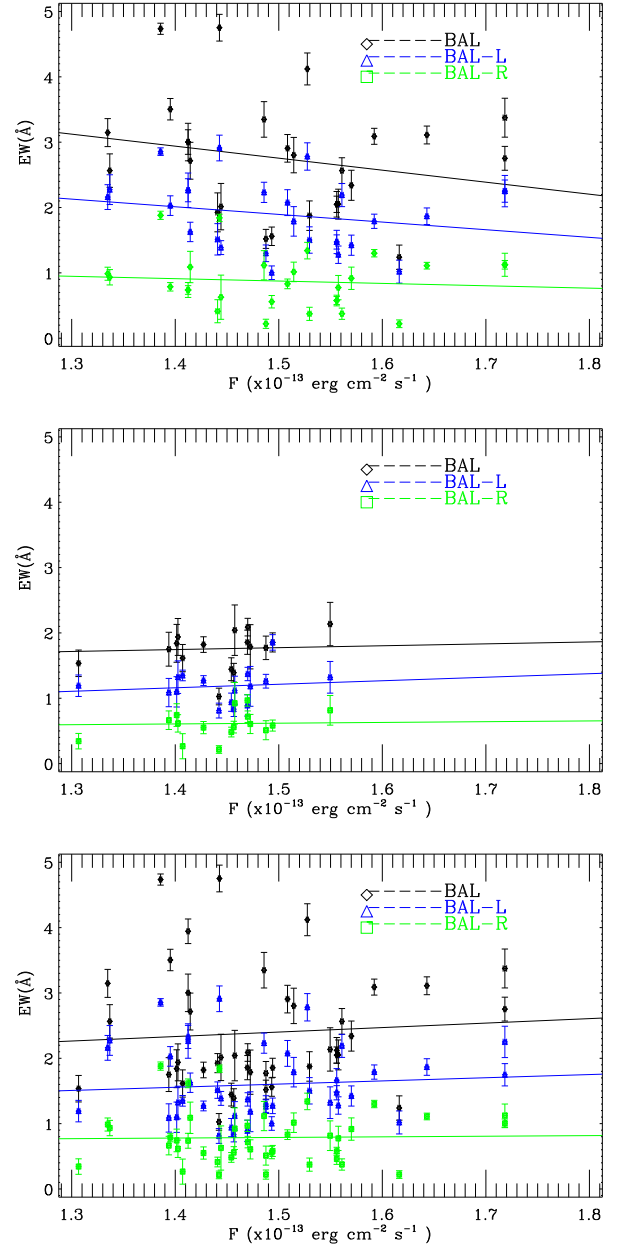


Figure 4. Plots of the EW of BALs versus the flux of the continuum for three samples. In each panel, the black, blue and green plots represent the BAL, BAL-L, and BAL-R, respectively. The solid lines are the corresponding linear regression fits. The top panel represents the variation sample (the MJD from 56426 to 56837). The middle panel represents the no variation sample (the MJDs are from 57038 to 57510). The bottom panel represents the whole sample, which includes all data of 44 epochs (the MJD from 56426 to 57510). For all the whole BALs, BAL-Ls, and BAL-Rs, the moderate anticorrelations between the EW of BALs and the flux of the continuum are found for the variation sample, while no correlation between them for both the no variation sample and the total sample.

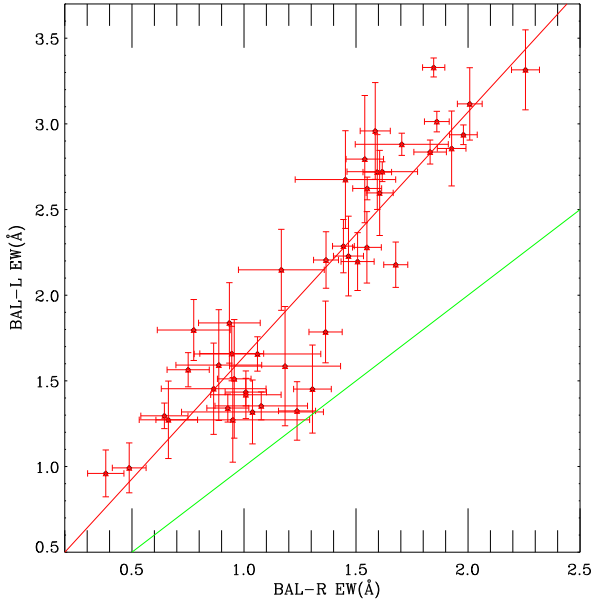


Figure 5. Comparison of the EWs between BAL-L and BAL-R. The red line is the linear regression fit for the data points. The green line is equal EWs for the two absorption troughs.

lines as well as remaining sky pixels (e.g. Lu & Lin 2018c). An example of the power-law continuum fit is shown in Fig. 1. We choose the wavelength range of 1200–2100 Å to obtain the flux of the continuum (F) and the corresponding uncertainty, the formulas are as follows:

$$F = \sum_i (\lambda_{i+1} - \lambda_i) \frac{1}{2} (F_{c_{i+1}} + F_{c_i}), \quad (1)$$

$$\sigma_F = \sqrt{\sum_i [\sigma_{F_{c_i}} (\lambda_{i+1} - \lambda_i)]^2}. \quad (2)$$

where F_c is the flux of the power-law continuum, σ_{F_c} is the uncertainty of the flux of the power-law continuum, λ is wavelength. The values of F_c and σ_{F_c} are listed in Table 1.

To fit the absorption lines, it is necessary to fit the pseudo-continuum spectra first. **Pseudo-continuum is a fitting curve along the initial spectrum but ignores the absorption lines.** We fit the continua of SDSS J1410+5412 by iteratively performing the cubic spline functions (e.g. Lu & Lin 2018a). To decrease the effects of absorption troughs as well as remaining sky pixels, we masked out the pixels which outside 3σ significance from the present fit. The continuum fitting is shown in Fig. 1. After that, we measured absorption lines in the spectra that have been normalized by the pseudo-continua.

As seen in Fig. 1, the whole region of C IV BAL is the combination of two parts (BAL-L and BAL-R). We thus employed two Gaussian functions to fit them, respectively. An example of the Gaussian fitting is displayed in Fig. 2. We measured the equivalent widths (EWs) of the absorption lines based on the Gaussian profile, and estimated the error of each Gaussian profile according to the corresponding flux

uncertainties via

$$\sigma_{EW} = \frac{\sqrt{\sum_i P^2(\lambda_i - \lambda_0) \sigma_{f_i}^2}}{(1 + z_{\text{abs}}) \times \sum_i P^2(\lambda_i - \lambda_0)} \Delta\lambda. \quad (3)$$

where P is the Gaussian function at center line λ_0 ; λ_i is the wavelength of data point; $\Delta\lambda$ is the spacing of adjacent points; σ_{f_i} is the uncertainty of the spectral flux of the normalization (Schneider et al. 1993). Then the total EW of the BAL are the sum of the two Gaussian profiles

$$EW_{BAL} = EW_{BAL-L} + EW_{BAL-R}, \quad (4)$$

and the error of the total EW is

$$\sigma_{EW_{BAL}} = \sqrt{\sigma_l^2 + \sigma_r^2}. \quad (5)$$

where EW_{BAL} , EW_{BAL-L} and EW_{BAL-R} are the EWs of BAL, BAL-L and BAL-R, respectively; $\sigma_{EW_{BAL}}$, σ_l and σ_r are the errors of BAL, BAL-L and BAL-R, respectively.

3 CORRELATION ANALYSIS AND DISCUSSION

Fig. 3 shows the EW measurements of BAL as a function of MJD. It is obviously that the BAL in J1410+5412 shows significant variation during MJD 56426 to 56837, while shows no significant variation during MJD 57038 to 57510. According to this phenomenon, we divided the multi-epoch spectra of J1410+5412 into two samples, i.e. the variation sample (MJD from 56426 to 56837) and the no variation sample (MJD from 57038 to 57510), and performed Spearman correlation to this two samples separately. We also performed a Spearman correlation to the total spectra sample. The statistical parameters are listed in Table 2. We plotted the EW of BALs versus the flux of the continuum in Fig. 4. The moderate anticorrelation between the EW of BALs and the flux of the continuum was confirmed by the Spearman rank correlation analysis for the variation sample, while no correlation between them for both the no variation sample and the total sample. When we divided each of the BALs into two parts, i.e. BAL-L and BAL-R, as we did in section 2, the correlation tests for the three sample also returned the same results with the total BALs (i.e. moderate anticorrelation between the EW of BAL-Ls/BAL-Rs and the flux of the continuum for the variation sample, while no correlation between them for both no variation sample and the total sample, see also Table 2 for details).

These results provide a new clue to understand the variation mechanism of the BAL in J1410+5412. Although there is substantial scatter in the plots, in the variation sample we find an anticorrelation between the the EW of BALs and the flux of the continuum, which serve as a direct evidence for the idea that BAL variability is driven mainly by changes in the gas ionization in response to the continuum variations. The moderate anticorrelation between the EW of BALs and the flux of the continuum of the variation spectra sample can roughly indicate the ionization states of absorbers, because photoionization simulations have shown that when the ionization parameter (U) increasing, the EWs of C IV rise till a peak, and decrease after then (e.g. Wang et al. 2015; He et al. 2017). Thus, the absorbers in J1410+5412 are at a relatively high ionization state.

Grier et al. (2015) also hold the same view with us. They drew their conclusions mainly based on the following two points. On the one hand, they found that variations occur across the whole trough rather than in some segments. On the other hand, the high-velocity C_{IV} BAL (Trough A in their paper) and the mini-BAL (Trough B in their paper) vary coordinately. We plotted the EW of BAL-L versus BAL-R in Fig. 5. The strong correlation between them was confirmed by the Spearman rank correlation analysis (see also Table 2). This result also confirms the coordinated variability between different parts of BAL trough in J1410+5412.

In summary, we found the correlation between the EW of BALs and the flux of the continuum of the variation spectra sample (MJD from 56426 to 56837), which confirms that the variation mechanism of the BAL in J1410+5412 is the ionization changes of the absorbers, as a response to the continuum variations. Our results support the conclusions made by Grier et al. (2015).

ACKNOWLEDGEMENTS

We are grateful to the editor and reviewer of this journal for their useful comments. Our work was supported by the Guangxi Natural Science Foundation (No. 2017GXNS-FAA198348). QYP acknowledges support from the Excellent Youth Foundation of Guangdong Province (Grant No. YQ2015128), and the Guangzhou Education Bureau (Grant No. 1201410593).

Funding for SDSS-III was provided by the Alfred P. Sloan Foundation, the Participating Institutions, the National Science Foundation and the US Department of Energy Office of Science. The SDSS-III website is <http://www.sdss3.org/>.

SDSS-III is managed by the Astrophysical Research Consortium for the Participating Institutions of the SDSS-III Collaboration, including the University of Arizona, the Brazilian Participation Group, Brookhaven National Laboratory, Carnegie Mellon University, University of Florida, the French Participation Group, the German Participation Group, Harvard University, the Instituto de Astrofísica de Canarias, the Michigan State/Notre Dame/JINA Participation Group, Johns Hopkins University, Lawrence Berkeley National Laboratory, Max Planck Institute for Astrophysics, Max Planck Institute for Extraterrestrial Physics, New Mexico State University, New York University, Ohio State University, Pennsylvania State University, University of Portsmouth, Princeton University, the Spanish Participation Group, University of Tokyo, University of Utah, Vanderbilt University, University of Virginia, University of Washington, and Yale University.

REFERENCES

Abolfathi B., et al., 2018, *ApJS*, **235**, 42
 Alam S., et al., 2015, *ApJS*, **219**, 12
 Allen J. T., Hewett P. C., Maddox N., Richards G. T., Belokurov V., 2011, *MNRAS*, **410**, 860
 Capellupo D. M., Hamann F., Shields J. C., Rodríguez Hidalgo P., Barlow T. A., 2011, *MNRAS*, **413**, 908
 Chen Z.-F., Pang T.-T., He B., Huang Y., 2018a, *ApJS*, **236**, 39

Chen Z.-F., et al., 2018b, *ApJS*, **239**, 23
 Crenshaw D. M., Kraemer S. B., George I. M., 2003, *ARA&A*, **41**, 117
 Dawson K. S., et al., 2013, *AJ*, **145**, 10
 Eisenstein D. J., et al., 2011, *AJ*, **142**, 72
 Farrah D., Lacy M., Priddey R., Borys C., Afonso J., 2007, *ApJ*, **662**, L59
 Ganguly R., Brotherton M. S., 2008, *ApJ*, **672**, 102
 Gibson R. R., Brandt W. N., Schneider D. P., Gallagher S. C., 2008, *ApJ*, **675**, 985
 Gibson R. R., et al., 2009, *ApJ*, **692**, 758
 Grier C. J., et al., 2015, *ApJ*, **806**, 111
 Hamann F., Barlow T. A., Junkkarinen V., 1997, *ApJ*, **478**, 87
 Hamann F., Kaplan K. F., Rodríguez Hidalgo P., Prochaska J. X., Herbert-Fort S., 2008, *MNRAS*, **391**, L39
 He Z., Wang T., Zhou H., Bian W., Liu G., Yang C., Dou L., Sun L., 2017, *ApJS*, **229**, 22
 Hemler Z. S., et al., 2019, *ApJ*, **872**, 21
 Hewett P. C., Wild V., 2010, *MNRAS*, **405**, 2302
 King A. R., 2010, in Maraschi L., Ghisellini G., Della Ceca R., Tavecchio F., eds, *Astronomical Society of the Pacific Conference Series Vol. 427, Accretion and Ejection in AGN: a Global View*. p. 315
 Lu W.-J., Lin Y.-R., 2018a, *MNRAS*, **474**, 3397
 Lu W.-J., Lin Y.-R., 2018b, *ApJ*, **862**, 46
 Lu W.-J., Lin Y.-R., 2018c, *ApJ*, **863**, 186
 Lu W.-J., et al., 2017, *MNRAS*, **468**, L6
 Lu W.-J., Lin Y.-R., Qin Y.-P., 2018, *MNRAS*, **473**, L106
 Misawa T., Charlton J. C., Eracleous M., Ganguly R., Tytler D., Kirkman D., Suzuki N., Lubin D., 2007a, *ApJS*, **171**, 1
 Misawa T., Eracleous M., Charlton J. C., Kashikawa N., 2007b, *ApJ*, **660**, 152
 Misawa T., Charlton J. C., Eracleous M., 2014, *ApJ*, **792**, 77
 Schneider D. P., et al., 1993, *ApJS*, **87**, 45
 Shen Y., et al., 2015, *VizieR Online Data Catalog*, **221**
 Shi X.-H., Jiang P., Wang H.-Y., Zhang S.-H., Ji T., Liu W.-J., Zhou H.-Y., 2016, *ApJ*, **829**, 96
 Smee S. A., et al., 2013, *AJ*, **146**, 32
 Springel V., Di Matteo T., Hernquist L., 2005, *ApJ*, **620**, L79
 Vivek M., Srianand R., Petitjean P., Mohan V., Mahabal A., Samui S., 2014, *MNRAS*, **440**, 799
 Wang T., Yang C., Wang H., Ferland G., 2015, *ApJ*, **814**, 150
 Weymann R. J., Morris S. L., Foltz C. B., Hewett P. C., 1991, *ApJ*, **373**, 23
 Wildy C., Goad M. R., Allen J. T., 2014, *MNRAS*, **437**, 1976

Table 1. The fitting data of BAL and the power-law continuum spectra.

MJD (Day)	S/N	EW_{BAL-L} (Å)	EW_{BAL-R} (Å)	EW_{BAL} (Å)	F ($10^{-13} \text{ erg cm}^{-2} \text{ s}^{-1}$)
56426	23.87	2.67±0.29	1.45±0.22	4.13±0.36	1.7184±0.0017
56660	27.32	2.96±0.28	1.59±0.07	4.54±0.29	1.5084±0.0013
56664	23.39	2.79±0.37	1.54±0.08	4.33±0.38	1.5297±0.0015
56683	29.40	2.60±0.25	1.61±0.06	4.20±0.26	1.7184±0.0010
56686	29.05	2.72±0.22	1.59±0.06	4.31±0.23	1.4409±0.0017
56697	28.84	2.94±0.06	1.98±0.06	4.92±0.08	1.3859±0.0011
56717	32.71	3.12±0.21	2.01±0.06	5.12±0.22	1.4427±0.0010
56720	32.05	3.32±0.23	2.26±0.06	5.57±0.24	1.4859±0.0011
56722	37.00	3.33±0.06	1.85±0.05	5.18±0.07	1.5376±0.0010
56726	31.22	3.01±0.06	1.86±0.06	5.56±0.08	1.3952±0.0011
56739	29.77	2.84±0.07	1.83±0.07	4.67±0.10	1.4124±0.0011
56745	29.96	2.62±0.07	1.55±0.06	4.17±0.09	1.5610±0.0013
56749	29.96	2.88±0.06	1.70±0.21	4.17±0.22	1.3368±0.0010
56751	31.51	2.86±0.22	1.93±0.06	4.78±0.23	1.4124±0.0011
56755	29.75	2.20±0.17	1.51±0.07	3.70±0.18	1.4442±0.0011
56768	32.17	2.72±0.06	1.62±0.16	4.34±0.17	1.3348±0.0009
56772	37.54	2.29±0.16	1.44±0.05	3.86±0.16	1.6430±0.0010
56780	30.48	2.28±0.21	1.55±0.06	3.83±0.22	1.4145±0.0010
56782	36.71	2.18±0.13	1.68±0.05	3.86±0.14	1.5922±0.0011
56795	30.16	2.23±0.23	1.47±0.07	3.69±0.24	1.5701±0.0012
56799	37.04	2.21±0.16	1.37±0.06	3.57±0.17	1.5560±0.0010
56804	29.50	1.27±0.23	0.66±0.13	1.94±0.26	1.6163±0.0013
56808	30.47	1.79±0.18	1.36±0.07	3.15±0.19	1.5575±0.0012
56825	33.75	2.15±0.24	1.17±0.19	3.31±0.30	1.5660±0.0011
56829	31.70	1.84±0.23	0.93±0.14	2.77±0.27	1.5145±0.0012
56833	31.71	1.80±0.18	0.78±0.16	2.57±0.24	1.4876±0.0012
56837	35.22	1.42±0.14	1.01±0.16	2.43±0.21	1.4932±0.0011
57038	25.30	1.66±0.16	0.95±0.14	2.60±0.21	1.4941±0.0013
57050	25.08	1.45±0.27	0.86±0.23	2.32±0.35	1.5496±0.0014
57067	22.59	1.43±0.08	1.01±0.09	2.44±0.12	1.4071±0.0014
57082	22.94	1.32±0.19	1.04±0.32	2.36±0.37	1.3067±0.0013
57106	24.77	1.34±0.08	0.93±0.09	2.29±0.16	1.1529±0.0012
57127	25.03	1.27±0.25	0.95±0.34	2.22±0.42	1.4575±0.0014
57135	25.95	1.51±0.35	0.96±0.07	2.47±0.35	1.4026±0.0012
57159	24.77	1.59±0.32	0.89±0.19	2.48±0.38	1.3938±0.0013
57166	26.58	1.59±0.35	1.18±0.25	2.77±0.43	1.4014±0.0012
57185	24.40	0.96±0.14	0.38±0.08	1.34±0.16	1.4422±0.0014
57196	26.86	1.30±0.07	0.64±0.11	1.94±0.13	1.4273±0.0012
57428	22.23	1.66±0.10	1.06±0.28	2.72±0.3	1.4876±0.0015
57435	25.29	0.99±0.15	0.49±0.08	1.50±0.18	1.4542±0.0013
57451	25.66	1.35±0.08	1.08±0.21	2.43±0.22	1.4725±0.0013
57463	23.50	1.45±0.26	1.31±0.08	2.76±0.27	1.4697±0.0014
57492	22.80	1.56±0.10	0.75±0.09	2.32±0.14	1.4700±0.0014
57510	26.29	1.32±0.17	1.24±0.08	2.56±0.19	1.4565±0.0014

This paper has been typeset from a $\text{\TeX}/\text{\LaTeX}$ file prepared by the author.

Table 2. Correlated parameters of EW versus F and EW versus EW for each sample.

	EW VS. F for MJD 56426-56837		EW VS. F for MJD 57038-57510		EW VS. F for All sample	
	r ^a	p ^b	r	p	r	p
BAL	-0.46	0.016	0.12	0.653	0.06	0.718
BAL-L	-0.47	0.014	0.25	0.333	0.08	0.622
BAL-R	-0.54	0.003	0.03	0.896	-0.01	0.952
EW VS. EW						
	r	p				
L-R	0.88	4.044×10^{-15}				

Notes.^aThe Spearman rank correlation coefficient.

^bThe significance level of the correlation coefficient.